

# スパイクニューロン回路の多彩な分岐現象の解析

桐川, 翔太 / KIRIKAWA, Shota

---

(出版者 / Publisher)

法政大学大学院理工学・工学研究科

(雑誌名 / Journal or Publication Title)

法政大学大学院紀要. 理工学・工学研究科編 / 法政大学大学院紀要. 理工学・工学研究科編

(巻 / Volume)

55

(開始ページ / Start Page)

1

(終了ページ / End Page)

6

(発行年 / Year)

2014-03-24

(URL)

<https://doi.org/10.15002/00010409>

# スパイクニューロン回路の多彩な分岐現象の解析

ANALYSIS OF VARIOUS BIFURCATION PHENOMENA IN SIMPLE SPIKING NEURON CIRCUITS

桐川 翔太

Shota KIRIKAWA

指導教員 斎藤利通

法政大学大学院理工学研究科電気工学専攻修士課程

This paper studies filter-induced bifurcation phenomena in simple spiking neuron models. Repeating integrate-and-fire switching between a periodic base signal and a threshold, the neuron model outputs spike-trains. The dynamics depends crucially on the shape of the base signal and we make the base signal by applying two kinds of filters to a square source signal. First, we apply the basic RC low-pass filter to the source signal. As a key parameter (time constant) varies, the shape of the base signal varies and the model can exhibit bifurcation phenomena of various periodic/chaotic spike-trains. Presenting a simple test circuit, typical phenomena are confirmed experimentally. Second, we apply the ideal low-pass filter to the source signal. The ideal filter cannot be realized by analog circuits and is an object in artificial numerical experiments. This filter causes ripple on the base signal (the Gibbs' phenomenon) and the model can have various co-existence spike-trains.

**Key Words :** *Bifurcation, Chaos, Spiking neurons, Spike-trains, Analog filters, Ideal filters*

## 1. Introduction

Spiking neurons have been studied extensively from both basic and practical viewpoints. Roughly speaking, the neurons can exhibit a variety of spike-trains based on the integrate-and-fire switching [1]-[3]. The analysis of the spike-trains is basic to consider information processing function [3]. It is also basic to develop spike-based applications including image processing [4], digital communications [5], analog-to-digital converters [6] [7] and neural prosthesis [8]. The spiking neurons are typical non-linear dynamical systems that can exhibit chaos [9] and bifurcation phenomena. Analysis of the phenomena is an important basic problem [10]-[16].

This paper studies filter-induced behavior of bifurcating neurons (BNs, [10]-[13]). The BN is a simple spiking neuron model. Repeating integrate-and-fire switching between a periodic base signal and a constant threshold, the BN can exhibit various spike-trains. The spike-trains can be analyzed precisely by a one-dimensional map of spike positions or phases. The dynamics of the BN depends crucially on shape of the base signal. We consider a method to vary the shape of the base signal by applying a filter to a square base signal. If the filter does not exist, the base signal is a periodic square wave and the BN cannot exhibit chaos and bifurcation. Although there exist various kinds of filters, we use two kinds of basic filters for simplicity. We then consider bifurcation phenomena for a parameter of the filter. In existing papers of the BN [10]-[16], bifurcation phenomena have been considered for a parameter of amplitude or frequency of the base signal.

First, we apply a simple RC low-pass filter (RCF) characterized by one key parameter corresponding to the time constant. As the key parameter varies, the shape of the base signal can vary and the BN can exhibit various periodic/chaotic spike-trains. Using the state equation of the RCF, the filtered base signal can be calculated without approximation and the bifurcation phenomena can be analyzed precisely. We have clarified that as the key parameter varies, the BN exhibits period doubling bifurcation to chaos and then to thin chaos via periodic windows. Presenting a simple test circuit, typical phenomena are confirmed experimentally.

Second, we apply the ideal low-pass filter (ILF) that corresponds to the finite terms approximation of the Fourier series. As is well known, the ILF cannot be realized by analog circuits and the ILF is an object in artificial numerical experiments. The ILF is characterized by one key parameter that gives the number of terms in the Fourier series approximation. Note that even if the number of terms is sufficiently large, the ILF causes ripple for the discontinuous source signal (the Gibbs' phenomenon). In the BN, the ripple can cause complicated co-existing periodic/chaotic phenomena. The BN exhibits either phenomenon depending on the initial state.

Motivations for studying the filter-induced phenomena are many, including the following three points. First, the key parameters of RCF and ILF have important practical meanings for variable shapes of the base signal. Second, the RCF-induced bifurcation is easy to implement and is convenient for precise analysis.

## 2. Bifurcating Neurons

Let us begin with introducing the BN dynamics [10]-[13]. Figure 1 shows the circuit model and switching dynamics of the BN. Integrating a constant current  $I > 0$ , the capacitor voltage  $v$  increases. When  $v$  reaches the threshold  $V_T$ , the BN outputs a spike  $Y = V_D$  and  $v$  is reset to the periodic base signal  $B(t)$  with period  $T$ . Repeating in this manner, the BN outputs a spike-train  $Y(t)$ . For simplicity, we assume that the inner resistor  $r_1$  is open, the inner resistor  $r_2$  is short and  $v$  is reset instantaneously without delay. The circuit dynamics is described by

$$\begin{cases} C \frac{dv}{dt} = I, & Y = -V_D & \text{for } v < V_T \\ v(t_+) = B(t_+), & Y(t) = V_D & \text{for } v(t) = V_T \end{cases} \quad (1)$$

Here we use the simple square base signal:

$$B(t) = B_s(t) = \begin{cases} -A & \text{for } 0 \leq t < T/2 \\ A & \text{for } T/2 \leq t < T \end{cases} \quad (2)$$

where  $B_s(t) = B_s(t+T)$  and  $0 < A < V_T$ . In the next section, this base signal is changed into various shapes by filtering. Using dimensionless variables and parameters

$$\begin{aligned} \tau &= \frac{t}{T}, \quad x = \frac{v}{V_T}, \quad y = \frac{Y + V_D}{2} \\ s &= \frac{IT}{CV_T}, \quad a = \frac{A}{V_T}, \quad b(\tau) = \frac{1}{V_T} B(T\tau); \end{aligned} \quad (3)$$

Equations (1) and (2) are transformed into

$$\begin{cases} \dot{x} = s, & y = 0 & \text{for } x < 1 \\ x(\tau_+) = b(\tau_+), & y(\tau) = 1 & \text{for } x(\tau) \geq 1 \end{cases} \quad (4)$$

$$b(\tau) = b_s(\tau) = \begin{cases} -a & \text{for } 0 \leq \tau < 1/2 \\ a & \text{for } 1/2 \leq \tau < 1 \end{cases}$$

where  $\dot{x} \equiv \frac{dx}{d\tau}$ ,  $b_s(\tau+1) = b_s(\tau)$  and  $0 < a < 1$ .

Let us derive the spike-position map (Smap) and spike-phase map (Pmap). The spike-train is characterized by spike positions and let  $\tau_n$  denote the  $n$ -th spike position. Since  $\tau_{n+1}$  is determined by  $\tau_n$ , we can define the Smap:

$$\tau_{n+1} = \tau_n - (b(\tau_n) - 1)/s \equiv F(\tau_n) \quad (5)$$

Note that  $F(\tau+1) = F(\tau)+1$  is satisfied. Introducing the phase variable  $\theta_n = \tau_n \bmod 1$ , we can define the Pmap:

$$\theta_{n+1} = f(\theta_n) \equiv F(\theta_n) \bmod 1 \quad (6)$$

The dynamics of the BN is integrated into the Pmap that is useful to analyze the bifurcation phenomena. Figure 2 illustrates examples of the Smap and Pmap for  $b(\tau) = b_s(\tau)$ . It should be noted that Equation (5) include the base signal  $b(\tau)$  and the dynamics of Pmap (and Smap) crucially depends on the shape of  $b(\tau)$ . However, in almost all works on the BN, the shape of  $b(\tau)$  is fixed. For example, Ref. [15] uses the sinusoidal base signal and considers bifurcation for the amplitude parameter. In this

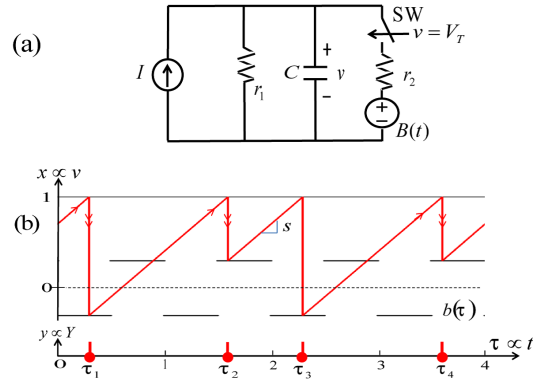


Figure 1 The bifurcating neuron. (a) circuit model, (b) integrate-and-fire dynamics for square base signal ( $s = 1$ ,  $a = 0.3$  and  $\lambda = 0$ ).

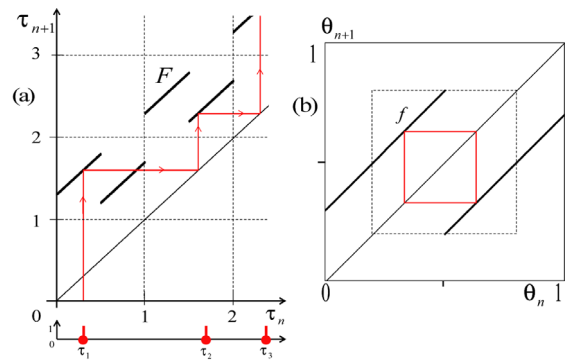


Figure 2 Examples of spike position map (a) and spike phase map (b) for  $(s, a) = (1, 0.3)$ .

paper, we construct the base signal by applying the LPF to the square waveform  $B_s(t)$  in Equation (2). If the filters do not exist, the BN has the square base signal  $B_s(t)$  and the slope of the Pmap is one ( $Df(\theta) = 1$ ) for almost all  $\theta$ : the Pmap cannot exhibit chaos and related bifurcation. Although there exist various kinds of LPFs, we consider two kinds of LPFs: the most basic RC low-pass filter (RCF) and ideal low-pass filter (ILF).

### 3. Base signal by RC low-pass filter

Here we apply the RCF to the source signal  $B_s(t)$ . Usually, such a base signal is described by Fourier series with transfer function of the RCF and finite-term approximation error is inevitable. In order to avoid the approximation error, we describe the base signal by state equation of the RCF:

$$RC_1 \frac{dv_c}{dt} = -v_c + B_s(t) \quad (7)$$

where the capacitor voltage  $v_c$  corresponds to the base signal. A test circuit of the BN with RCF is shown in (2). Using the dimensionless variables and parameters

$$\tau = \frac{t}{T}, \quad x_c = \frac{v_c}{V_T}, \quad \lambda = \frac{RC_1}{T} \quad (8)$$

Equation (7) is transformed into

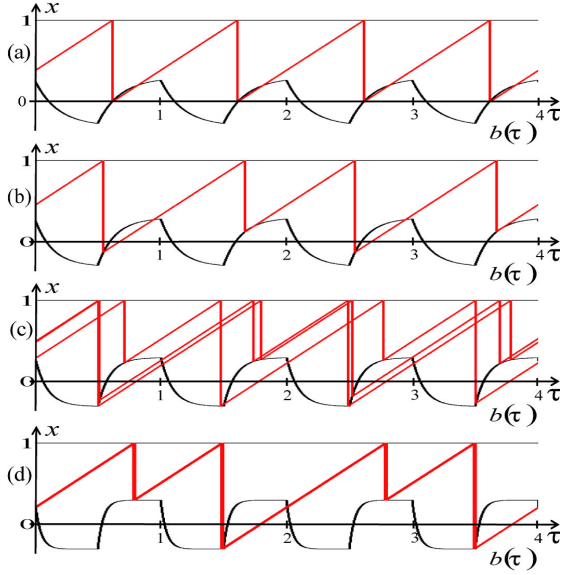


Figure 3 Typical waveforms for  $(s, a) = (1, 0.3)$ . (a) periodic waveform with period 1 for  $\lambda = 0.18$ , (b) periodic waveform with period 2 for  $\lambda = 0.14$ , (c) chaotic waveform for  $\lambda = 0.095$ , (d) thin chaotic waveform for  $\lambda = 0.045$ .

$$\lambda \dot{x}_c = -x_c + b_s(\tau) \quad (9)$$

After simple calculation, we obtain the steady state solution that is the base signal:

$$b(\tau) = \begin{cases} (x_0 + a)e^{-\tau/\lambda} - a & \text{for } 0 \leq \tau < 1/2 \\ (-x_0 - a)e^{-(\tau-1/2)/\lambda} + a & \text{for } 1/2 \leq \tau < 1 \end{cases} \quad (10)$$

$$x_0 = \frac{a(1 - e^{-1/2\lambda})}{1 + e^{-1/2\lambda}}$$

where  $b(\tau) = b(\tau + 1)$  and  $x_0$  is the initial value for the steady state solution. Using Equation (10) and the Pmap, we can analyze the dynamics precisely without approximation. We use  $\lambda$  as the key parameter of the RCF.

### (1) Basic bifurcation phenomena

We investigate basic bifurcation for parameter  $\lambda$  in decrease-ward for convenience. Other parameters are fixed:  $(s, a) = (1, 0.3)$ . As  $\lambda$  decreases to zero, the shape of base signal is changed from triangular-like waveform (Fig. 3 (a)) to square waveform (Fig. 1 (b)). According to the change of the shape, the BN can exhibit various phenomena as shown in Fig. 3: periodic waveform with period 1 in (a), periodic waveform with period 2 in (b) and chaotic waveform in (c).

In order to consider the phenomena, we give several definitions. A point  $p$  is said to be a period- $k$  point if  $f^k(p) = p$  and  $f^l(p) \neq p$  for  $0 < l < k$  where  $f^l = f(f^{l-1})$ . A period-1 point is referred to as a fixed point. Let  $Df^k(p)$  denotes derivative of  $f^k$  by  $\theta$  at  $p$ . A period- $k$  point is said to be stable, critical and unstable if  $|Df^k(p)| < 1$ ,  $|Df^k(p)| = 1$  and  $|Df^k(p)| > 1$ , respectively. The stable period- $k$  point corresponds to periodic

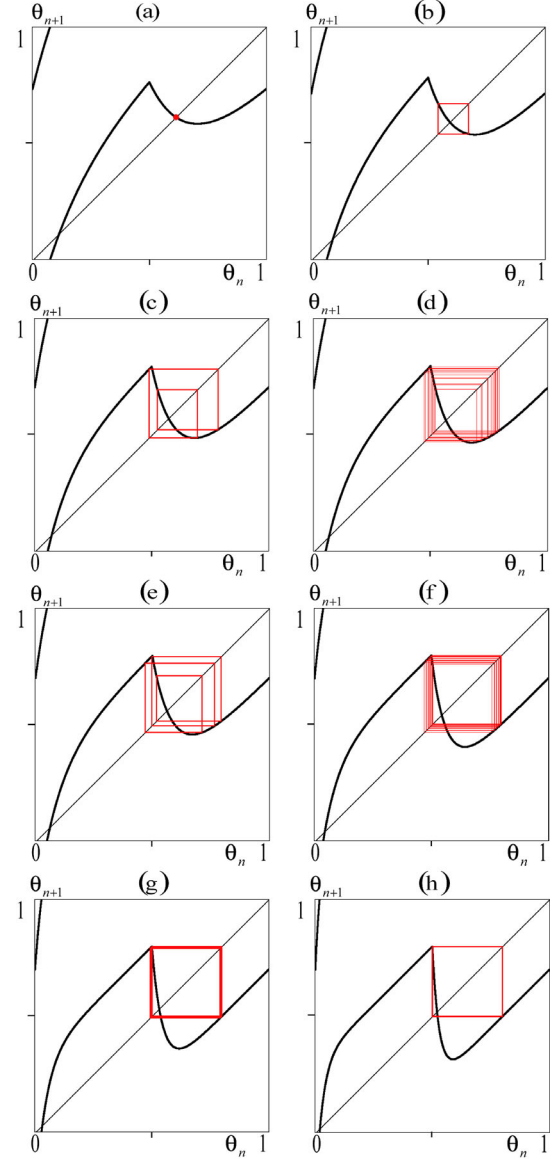


Figure 4 Typical phase maps for  $(s, a) = (1, 0.3)$  (a) stable fixed point for  $\lambda = 0.18$ , (b) stable period-2 orbit for  $\lambda = 0.14$ , (c) Stable period-4 orbit for  $\lambda = 0.106$ , (d) chaotic orbit for  $\lambda = 0.095$ , (e) stable period-6 orbit for  $\lambda = 0.09$ , (f) chaotic orbit for  $\lambda = 0.064$ , (g) thin chaotic orbit for  $\lambda = 0.045$ , (h) thin chaotic orbit for  $\lambda = 0.029$ .

waveform with period  $k$  of  $x$ . A sequence of period- $k$  points,  $\{f(p), \dots, f^k(p)\}$  is said to be a period- $k$  orbit.

Figure 4 shows typical Pmaps. For  $\lambda = 0.18$ , the Pmap exhibits stable fixed point  $p$  corresponding to periodic waveform with period 1 of  $x$ . As  $\lambda$  decreases, we can see the period-doubling bifurcation set characterized by  $Df(p) = -1$ . The fixed point  $p$  is changed into stable period-2 orbit as shown in Fig. 4 (b). As  $\lambda$  decreases further, the period-2 orbit is changed into the period-4 orbit in (c) and then to chaotic orbit in (d). This is the period-doubling bifurcation for the key parameter  $\lambda$  of the RCF. Although there exist various systems in which

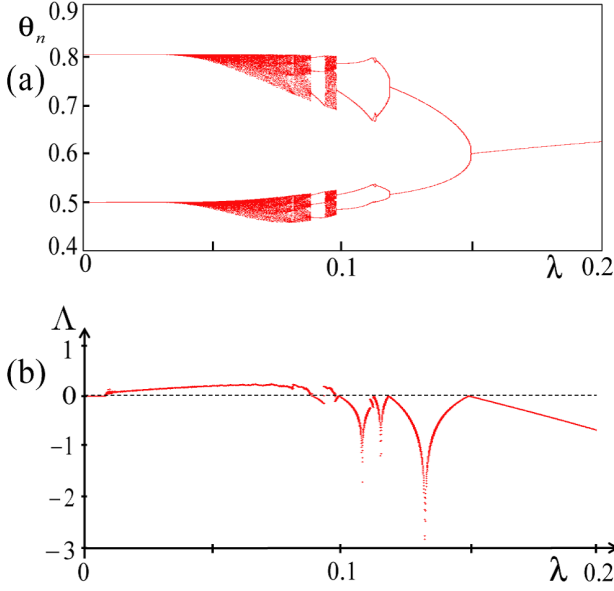


Fig 5 Bifurcation for  $\lambda$  and  $(s, a) = (1, 0.3)$ . (a) Bifurcation diagram, (b) Lyapunov exponent.

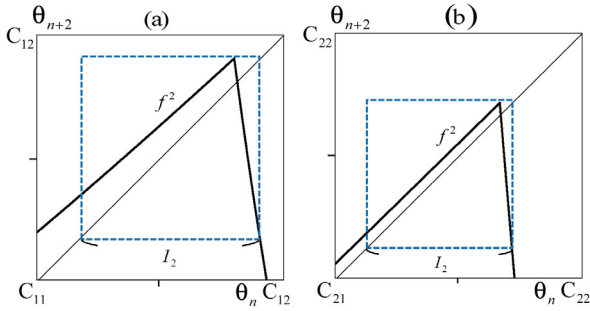


Fig 6 Two-fold composition of the Pmap around the chaotic orbit for  $(s, a) = (1, 0.3)$ . (a)  $\lambda = 0.064$  ( $C_{11} = 0.46, C_{12} = 0.51$ ), (b)  $\lambda = 0.045$  ( $C_{21} = 0.49, C_{22} = 0.505$ ).

period-doubling bifurcation can be observed, Fig. 4 shows the first filter-induced period-doubling bifurcation. Figure 5 (a) shows the corresponding bifurcation diagram for  $\lambda$ .

The chaotic orbit in (d) is changed into stable period-6 orbit in (e) that is in periodic window in Fig. 5 (a). As  $\lambda$ , the orbit is changed into chaotic orbit (f), the band of the chaotic orbits becomes thin as shown in (g) and (h), and then to period-2 orbit in Fig. 2 (b). The period-2 orbit  $\{f(p), f^2(p)\}$  for  $\lambda = 0$  is characterized by  $Df^2(p) = 1$  and is critical. Figure 6 shows 2-fold composition of Pmap  $f^2$  for thin chaos where we can confirm existence of invariant interval  $I_2$  such that  $f^2(I_2) \subseteq I_2$  on which the Pmap exhibits chaotic phenomenon.

In order to evaluate the orbits, we have calculated the Lyapunov exponent for  $\lambda$ :

$$\Lambda = \sum_{n=1}^M \ln |Df(x_n)| \quad (11)$$

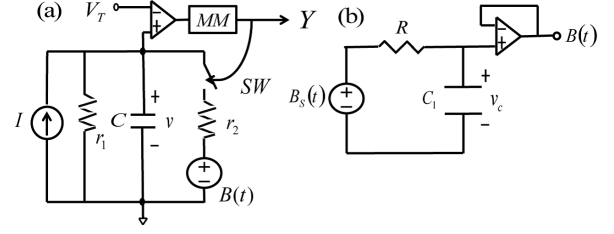


Fig 7 Circuit model (a) Bifurcating neuron (b) RC LPF.

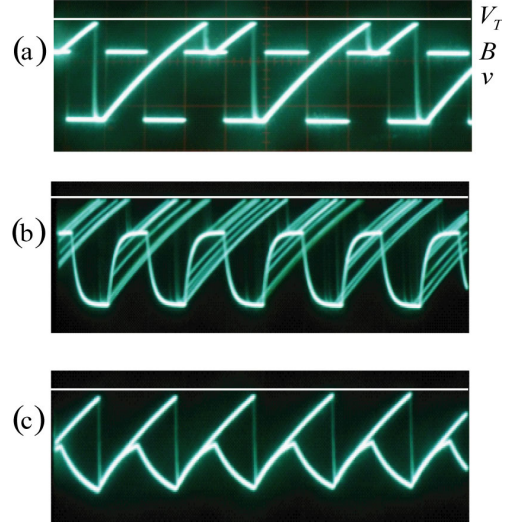


Fig 8 Measurement of typical phenomena corresponding to Fig. 3. horizontal =  $t$  [0.5ms/div.], vertical =  $v$  [1V/div.],  $C \doteq 0.022[\mu\text{F}]$ ,  $J \doteq 7.0 \text{ E } -2[\text{mA}]$ ,  $r_1 \doteq 90[\text{k}\Omega]$ ,  $r_2 \doteq 0.09[\text{k}\Omega]$ ,  $V_T \doteq 1.4[\text{V}]$ ,  $A \doteq 0.8[\text{V}]$ ,  $T \doteq 1[\text{ms}]$ ,  $C_1 \doteq 0.01[\mu\text{F}]$ , ( $s \doteq 1.45$ ,  $a \doteq 0.57$ ) (a) periodic waveform with period 2 for  $R \doteq 0[\text{k}\Omega]$  ( $\lambda = 0$ ) (b) chaotic waveform for  $R \doteq 7[\text{k}\Omega]$  ( $\lambda = 0.07$ ) (c) periodic waveform with period 1 for  $R \doteq 36[\text{k}\Omega]$  ( $\lambda = 0.36$ ).

where we have used  $M = 10^4$  for which convergence has been confirmed for almost all values of  $\lambda$ . The derivative  $Df$  can be calculated using the exact piecewise solution in Equation (10):

$$Df(\theta) = \begin{cases} 1 + \frac{x_0 + a}{\lambda} e^{-\frac{\theta}{\lambda}} & \text{for } 0 \leq \theta < 1/2 \\ 1 - \frac{x_0 + a}{\lambda} e^{-\frac{2\theta-1}{2\lambda}} & \text{for } 1/2 \leq \theta < 1 \end{cases} \quad (12)$$

Chaotic orbit is characterized by positiveness of the Lyapunov exponent [9] ( $\Lambda > 0$ ). Also, a periodic orbit is stable if  $\Lambda < 0$ . Period doubling bifurcation set ( $Df(p) = -1$ ) and critical periodic points ( $|Df^k(p)| = 1$ ) give  $\Lambda = 0$ . In Fig. 5, we can confirm  $\Lambda > 0$  for the thin chaotic orbit and  $\Lambda = 0$  for the period-doubling bifurcation set. As  $\lambda$  approaches to zero, the Pmap approaches to the rotation of the unit circle with rotation number 0.5 that exhibits critical period-2 orbit with  $\Lambda = 0$ .

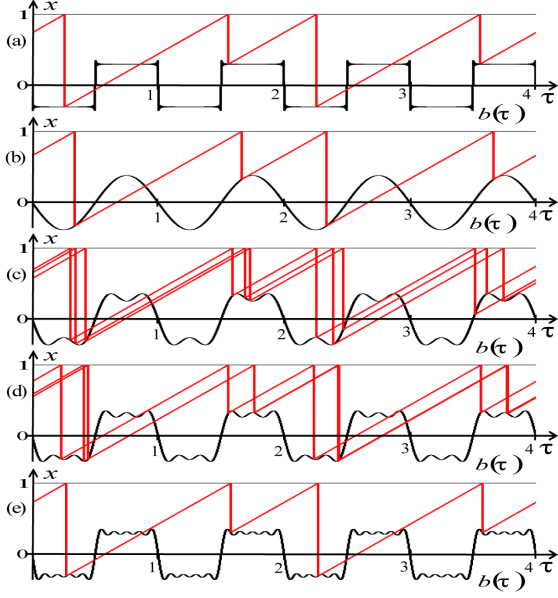


Fig. 9 Typical waveforms of BN with ILF corresponding to Fig. 10. (a) periodic waveform for  $N = 99$ , (b) periodic waveform for  $N = 1$ , (c) chaotic waveform for  $N = 3$ , (d) chaotic waveform for  $N = 5$ , (e) periodic waveform for  $N = 9$ .

## (2) Experiments

Figure 7 shows the test circuit for the laboratory experiments, The current source  $I$  with parallel inner resistor  $r_1$  can be realized by the equivalent circuit of voltage source of  $V = r_1 I$  with series inner resistor  $r_1$ . The base signal  $B(t)$  is given by filtering the square voltage sources  $B_s(t)$  and  $r_2$  is its inner resistor. Below the threshold  $V_T$ , the capacitor voltage  $v$  increases. If  $v$  reaches  $V_T$  then the comparator triggers a monostable multi-vibrator (MM) to output a spike  $Y = V_D$ . The spike closes a switch  $SW$  and  $v$  is reset to the base signal  $B(t)$ . The dynamics is described by

$$C \frac{dv}{dt} = \begin{cases} -\frac{1}{r_1}v + J & \text{for } SW = \text{off} \\ -\left(\frac{1}{r_1} + \frac{1}{r_2}\right)v + J + \frac{1}{r_2}B(t) & \text{for } SW = \text{on} \end{cases} \quad (13)$$

For simplicity, we use approximation:  $1/r_1 \rightarrow \infty$ ,  $r_2 \rightarrow 0$ , and  $I = J(1 - \exp^{-1})^{-1}$ . In this case, Equation (13) can be approximated by Equation (1) that is transformed into Equation (4) using dimensionless variables and parameters in Equations (3) and (8). Fabricating the breadboard prototype of the circuit, we have confirmed typical phenomena as shown in Fig. 8.

## 4. Base signal by ideal low-pass filter

The ILF is characterized by the transfer function:

$$H(\omega) = \begin{cases} 1 & \text{for } |\omega| \leq \omega_c \\ 0 & \text{for } |\omega| > \omega_c \end{cases} \quad (14)$$

<sup>1</sup>the slope of line connecting  $(0, 0)$  and  $(r_1 C, v(r_1 C))$

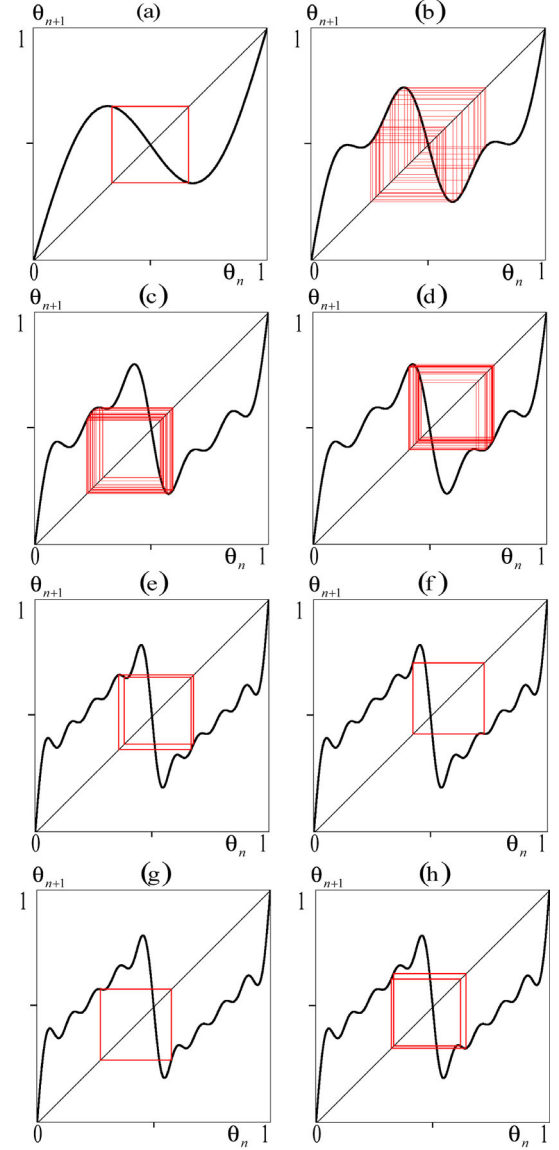


Fig. 10 Typical phase maps for  $(s, a) = (1, 0.3)$ . (a) stable period-2 orbit for  $N = 1$ , (b) chaotic orbit for  $N = 3$ , (c)&(d) coexisting chaotic orbits for  $N = 5$ , (e) to (h) co-existing stable periodic orbits for  $N = 9$ : (e) two period-2 orbits and (f) two period-4 orbits.

where  $\omega_c$  is the cut-off frequency and corresponds to  $1/RC_1$  of the RCF. Applying the ILF to the square signal  $B_s(t)$ , we obtain the base signal. As is well-known, the ILF cannot be realized by analog circuit because its impulse response contradicts the law of cause and effect. Hence we consider the ILF as an object in artificial numerical experiments. Using the dimensionless variables and parameters

$$\nu = \omega T, \quad \nu_c = \omega_c T,$$

we obtain the dimensionless transfer function

$$h(\nu) = \begin{cases} 1 & \text{for } |\nu| \leq \nu_c \\ 0 & \text{for } |\nu| > \nu_c \end{cases} \quad (15)$$

Applying this to the dimensionless square signal  $b_s(\tau)$ , we obtain the dimensionless base signal

$$\begin{aligned} b(\tau) &= \sum_{n=1}^{\infty} h(2\pi n) b_n \sin 2\pi n \tau \\ &= \sum_{n=1}^N b_n \sin 2\pi n \tau \quad \text{for } 2\pi N \leq \nu_c < 2\pi(N+1) \end{aligned} \quad (16)$$

where  $b_n$  are the Fourier sine coefficients of  $b_s(\tau)$ :

$$b_n = \begin{cases} -\frac{4a}{n\pi} & \text{for odd } n \\ 0 & \text{for even } n \end{cases}$$

It should be noted in Equation (16) that  $2\pi N \leq \nu_c < 2\pi(N+2)$  gives the same waveform of  $b(\tau)$  for odd  $N$  and the number of terms  $N$  determines  $b(\tau)$ . We use the odd  $N$  as the key parameter of the ILF. Figure 9 shows typical waveforms. As  $N$  increases, the base signal approaches  $b_s(\tau)$  in principle. However, even if  $N$  is sufficiently large, ripple is inevitable for the discontinuous waveform  $b_s(\tau)$  (the Gibb's phenomenon, see Fig. 9 (a)). Such ripple corresponds to many extremes in the Pmap and causes very complicated co-existence phenomena. Since analysis of such phenomena is hard, we focus on several basic cases as shown in Figs. 9 (except for (a)) and 10.

For  $N = 1$ , the base  $b(\tau)$  is pure sinusoidal, the BN exhibits periodic waveform with period 1 and the Pmap in (a) has one stable fixed point. For  $N = 3$ , the third harmonics occurs and the BN exhibits chaotic behavior as suggested in the Pmap in (b). As  $N$  increases, ripple of  $b(\tau)$  increases and the BN becomes to have coexisting phenomena for initial state. For  $N = 5$ , the Pmap has two symmetric chaotic orbits as shown in Fig. 10 (c) and (d). The BN exhibits either chaotic orbit depending on the initial state. For  $N = 9$ , we have confirmed four co-existing periodic orbits as shown in Fig. 10 (e) to (h): two symmetric period-2 orbits and two symmetric period-4 orbits. As  $N$  increases, the Pmap can have many co-existing attractors and related bifurcation phenomena seem to be very complicated. It suggests that the finite-term Fourier approximation can cause complex dynamics. However, its systematic analysis is hard.

## 5. Conclusions

Filter-induced bifurcation phenomena of the BN have been studied in this paper. First, the base signal is given by the simple RCF. As the key parameter decreases, the BN exhibits bifurcation phenomena of periodic/chaotic spike-trains. These bifurcations can be analyzed precisely using the Pmap and state equation of the base signal. Typical phenomena are confirmed experimentally in a simple test circuit. Second, the base signal is given by the ILF that causes the Gibb's phenomenon. As the key parameter varies, the ILF causes various ripples on the base signal and the BN can exhibit complicated co-existence state of various chaotic/periodic spike-trains.

Future problems are many, including detailed analysis of the RCF-induced bifurcation phenomena, detailed analysis of typical phenomena in the BN with ILF, application of various filters, analysis of the pulse-coupled networks of the BNs and engineering applications.

Third, the ILF-induced bifurcation is basic to consider complex dynamics caused by the finite terms approximation. It should be noted that such filter-induced complicated phenomena of spike-trains have not been studied in existing papers.

## 参考文献

- 1) J. P. Keener and F. C. Hoppensteadt and J. Rinzel, Integrate-and-fire models of nerve membrane response to oscillatory input, *SIAM J. Appl. Math.*, 41, pp. 503-517, 1981.
- 2) R. E. Mirollo and S. H. Strogatz, Synchronization of pulse-coupled biological oscillators, *SIAM J. Appl. Math.*, 50, pp. 1645-1662, 1990.
- 3) E. M. Izhikevich, Simple Model of Spiking Neurons, *IEEE Trans. Neural Networks*, 14, 6, 1569-1572, 2003.
- 4) S. R. Campbell, D. Wang, and C. Jayaprakash, Synchrony and desynchrony in integrate-and-fire oscillators, *Neural Comput.*, 11, pp. 1595-1619, 1999.
- 5) N. F. Rulkov, M. M. Sushchik, L. S. Tsimring and A. R. Volkovskii, Digital communication using chaotic-pulse-position modulation, *IEEE Trans. Circuits Syst. I*, 48, 12, 1436-1444, 2001.
- 6) H. Hamanaka, H. Torikai and T. Saito, Quantized spiking neuron with A/D conversion functions, *IEEE Trans. Circuits Syst. II*, 53, 10, pp. 1049-1053, 2006.
- 7) H. Torikai, A. Tanaka and T. Saito, Artificial Spiking Neurons and Analog-to-Digital-to-Analog Conversion, *IEICE Trans. Fundamentals*, E91-A, 6, pp. 1455-1462, 2008.
- 8) H. Torikai and T. Nishigami, An artificial chaotic spiking neuron inspired by spiral ganglion cell: parallel spike encoding, theoretical analysis, and electronic circuit implementation, *Neural Networks*, 22, 664-673, 2009.
- 9) E. Ott, *Chaos in dynamical systems*, Cambridge, 1993.
- 10) R. Perez and L. Glass, Bistability, period doubling bifurcations and chaos in a periodically forced oscillator, *Phys. Lett.*, 90A, 9, 441-443, 1982.
- 11) G. Lee and N. H. G., Farhat, The bifurcating neuron network 1, *Neural networks*, 14, 115-131, 2001.
- 12) E. D. M. Hernandez, G. Lee and N. H. Farhat, Analog realization of arbitrary one-dimensional maps, *IEEE Trans. Circuits Syst. I*, 50, 12, pp. 1538-1547, 2003.
- 13) H. Torikai, T. Saito and W. Schwarz, Synchronization via multiplex pulse-train, *IEEE Trans. Circuits Syst. I*, 46, 9, 1072-1085, 1999.
- 14) Y. Kon'no, T. Saito and H. Torikai, Rich dynamics of pulse-coupled spiking neurons with a triangular base signal, *Neural Networks*, 18, pp. 523-531, 2005.
- 15) H. Hamanaka, H. Torikai and T. Saito, Analysis of composite dynamics of two bifurcating neurons, *IEICE Trans. Fundamentals*, E88-A, 2, pp. 561-567, 2005.
- 16) K. Hisamatsu and T. Saito, Basic dynamics of simple delay-coupled bifurcating neurons, *IEICE Trans. Fundamentals*, E94-A, 3, pp. 1006-1009, 2011.